ACS Photonics

pubs.acs.org/journal/apchd5

Article

Quasi-Bound States in the Continuum of Localized Spoof Surface Plasmons

Si-Qi Li, Chao-Hai Du,* Li-Zheng Yin, Zi-Chao Gao, and Fan-Hong Li

Cite This: https://doi.org/10.1021/acsphotonics.2c00673

Read Online

ACCESS | Metrics & More | Article Recommendations

ABSTRACT: Localized spoof surface plasmons (LSSPs) have favorable characteristics of subwavelength confinement and nearfield enhancement but suffer from relatively low-quality factors (*Q*-factors), partly because of radiation loss. In this study, quasi-bound states in the continuum (quasi-BICs) of the LSSPs with high *Q*-factors are realized on a metasurface with eccentric circular grating as the unit when a plane wave is incident normally. Owing to the broken symmetry, LSSPs $TE_{2,1}$ and above turn into quasi-BICs from true-BICs and arise with weak energy leakage, which have the advantage of a high *Q*-factor. The behavior for the *Q*-factor of a quasi-BIC as a function of the asymmetry parameter is investigated. An experiment was carried out, and the results were in good agreement with the simulation ones. This work greatly reduces the radiation loss of the LSSPs and provides some inspiring applications of the LSSPs, such as remote detection, high-precision spectroscopy, and wireless sensing.

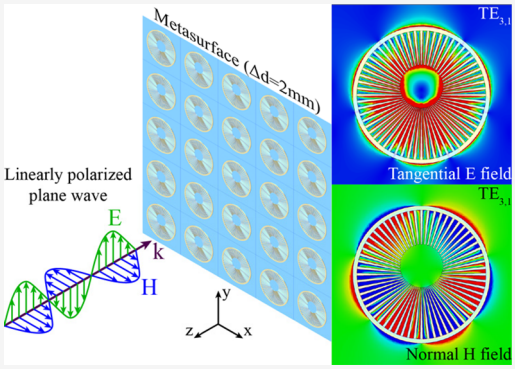

KEYWORDS: *quasi-bound states in the continuum, localized spoof surface plasmons, high Q-factors, metasurfaces, metamaterials*

INTRODUCTION

Localized surface plasmons (LSPs) have attracted extensive attention because of their characteristics of subwavelength confinement and nearfield enhancement in the optical band,[1−3] which have many applications in near-field optics, surface-enhanced spectroscopy, photovoltaics, and so forth. To expand the behaviors of the natural LSPs to microwave band, localized spoof surface plasmons (LSSPs) have been proposed and textured closed surfaces have been demonstrated to support the LSSPs.[4−10] They are well-qualified candidates for sensors,[11−14] bandpass filters,[15] invisibility cloaks,[16−18] orbital angular momentum (OAM) antennas,[19,20] isolators,[21] planar waveguides,[22] and so forth. However, the LSSP resonators are found to have the defect of a relatively low-quality factor (*Q*-factor) because of the material loss and the radiation loss. The former is inevitable, but fortunately, the latter can be greatly reduced in quasi-bound states in the continuum (quasi-BICs) from a distortion of symmetry-protected bound states in the continuum (BICs).

BICs, which exist in ideal (infinite and lossless) structures, lie inside the continuum but are perfectly confined without any radiation and cannot be excited by plane waves from infinity.[23] They have zero resonance widths and infinite *Q*-factors. They are mainly divided into two kinds: parameter-tuning BICs and symmetry-protected BICs.[23] Symmetry-protected BICs are attributed to the rotational symmetry of a system, which can be transformed into quasi-BICs by breaking the symmetry.[24,25] The *Q*-factors and the resonance widths of the quasi-BICs become finite, but because of the weak leakage, the *Q*-factors are relatively high. There have been some asymmetric periodic structures as the units of the metasurfaces that support the quasi-BICs, such as asymmetric tilted bars, dielectric nanodisks, circular split-rings, cubic resonators, and square split-rings.[26−37] They bring inspirations for the realization of the quasi-BICs of LSSPs and provide effective solutions for the LSSPs with high *Q*-factors. Therefore, eccentric circular grating formed by symmetry breaking is proposed as the unit of the metasurface.

In this study, quasi-BICs of the LSSPs are discovered. When a plane wave from infinity is incident normally on a metasurface with concentric circular grating as the unit, only LSSPs $TE_{1,1}$ mode can be excited; LSSPs $TE_{2,1}$ and above are true-BICs protected by rotational symmetry, which are completely decoupled from the plane wave and cannot be excited. Therefore, eccentric circular grating is proposed as the unit of the metasurface. Because of the broken symmetry, the LSSPs $TE_{2,1}$ and above turn into quasi-BICs, are coupled to

Received: May 4, 2022

the plane wave, and can be excited. Their Q-factors are relatively high because the energy leakage is weak. The Q-factor is inversely proportional to the square of the eccentricity of the circular grating. An experiment in the microwave band was carried out and the extremely sharp spectral resonances of the quasi-BICs of the LSSPs were observed, which is in good agreement with the numerical simulation.

SIMULATION RESULTS

Concentric and eccentric circular gratings are the basic units of the metasurfaces, and their schematics are shown in Figure 1a, b. The eccentric circular grating is formed by translating the inner circle of the concentric circular grating, and the displacement is Δd. Here, R_1 = 5 mm, R_2 = 15 mm, R_3 = 16 mm, h = 10 mm, b = 1 mm, a/d = 0.4, and N = 60. The metasurfaces are two-dimensional infinite in the x and y directions, and the period of the unit is 42 mm. The linearly polarized plane wave is incident normally on the metasurfaces, that is, the wavefront is parallel to the metasurfaces, and the wave vector is vertical to the metasurfaces (Figure 1c). For the metasurface with eccentric circular grating as the unit, the direction of the electric field of the wave is the same as the direction of the displacement Δd. (Other polarization directions are discussed in detail in the "Discussion" Section.)

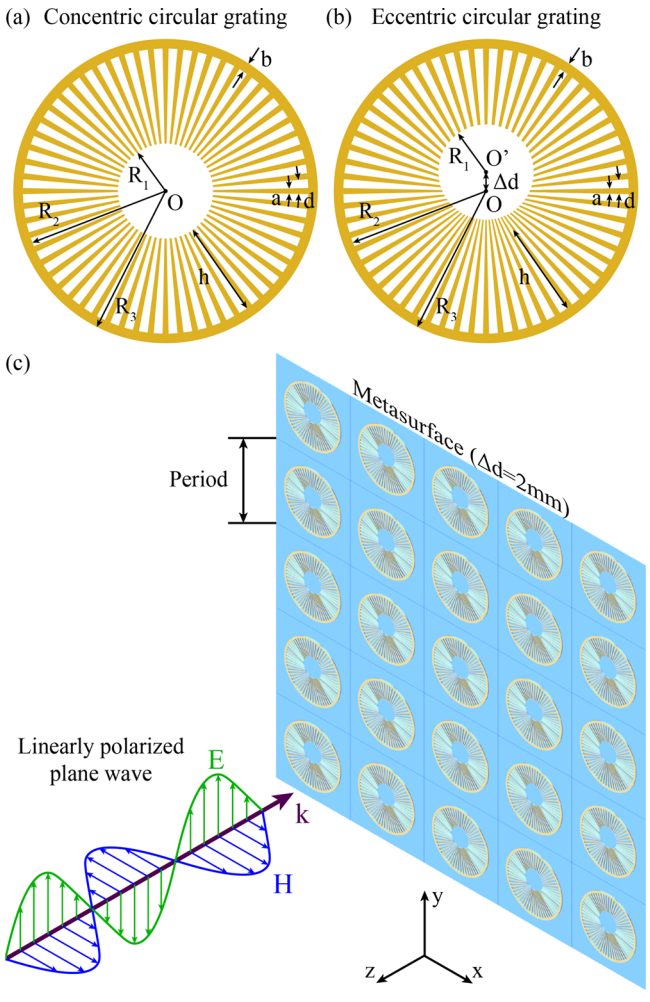

Figure 1. (a) Schematic of the concentric circular grating. The inner and outer circles are concentric. R_1 is the radius of the inner circle, R_2 is the radius of the outer circle, and R_3 is the radius of the edge. h (= $R_2 - R_1$) is the depth of the grating, b (= $R_3 - R_2$) is the width of the edge. a/d is the duty cycle of the grating. N is the number of the teeth. (b) Schematic of the eccentric circular grating. The inner and outer circles are eccentric, and the distance between their centers is Δd. (c) Configuration of the metasurface with eccentric circular grating as the unit. The linearly polarized plane wave is incident normally on the metasurface. The direction of the electric field is the same as the direction of Δd, that is, the electric field is along the y axis and the magnetic field is along the x axis.

The numerical simulation was carried out with CST Microwave Studio frequency domain solver. A tetrahedral mesh was chosen, an open boundary was set in the z direction, and a unit cell boundary was set in the x and y directions. An electric field monitor and a magnetic field monitor were placed. A perfect electrical conductor (PEC) was taken as the material of the metal, and loss-free Rogers RO4003C with a thickness of 0.508 mm and relative permittivity of 3.38 was set as the dielectric substrates. The material losses of the metal and the dielectric substrates were neglected. Therefore, the metasurfaces were under the ideal (infinite and lossless) conditions for BICs.

True-BICs of LSSPs. When a plane wave from infinity is incident normally on the metasurface with the concentric circular grating as the unit, only LSSPs fundamental $TE_{1,1}$ mode can be excited and high-order modes vanish. The transmission and reflection spectra are shown in Figure 2a, the dip in the transmission spectrum corresponds to the $TE_{1,1}$ mode. This phenomenon is related to the topological properties of the LSSP modes. The LSSPs $TE_{n,1}$ modes ($n \geq 2$) have C_n rotational symmetry because they still look the same after rotating $360/n°$ around their centers, and n is the azimuthal mode index. Therefore, they are true-BICs protected by rotational symmetry, which are completely decoupled from the plane wave and are perfectly confined without any radiation loss, and as a result, they cannot be excited by the plane wave. However, the LSSPs $TE_{1,1}$ mode (n = 1) has no rotational symmetry because it looks the same only after rotating 360°. Therefore, it is a leaky mode rather than a BIC and can be easily excited. The LSSPs is a transverse electric (TE) mode, that is, the electric field is parallel to the grating and the magnetic field is vertical to the grating. The tangential electric field and normal magnetic field of the $TE_{1,1}$ mode are shown in Figure 2b, c; they present the typical pattern of the LSSPs.

Quasi-BICs of LSSPs. In order to enable the LSSPs $TE_{2,1}$ and above to be coupled to and excited by the plane wave, we break the rotational symmetry of the concentric circular grating by translating the inner circle a displacement Δd and obtain the eccentric circular grating. Here, we select Δd = 2 mm as an example. When the identical plane wave is incident normally on the metasurface with the eccentric circular grating as the unit, all the LSSPs modes can be excited, among which the LSSPs $TE_{2,1}$ and above are quasi-BICs and are labeled in red in Figure 3a. Because the rotational symmetry has been broken, the LSSPs $TE_{2,1}$ and above transform into quasi-BICs from the true-BICs, which are coupled to the plane wave and arise from the distortion. The electromagnetic field distributions of the $TE_{1,1}$, $TE_{2,1}$, and $TE_{3,1}$ modes are shown in Figure 3b–g; although they are a little bit distorted, they still present the patterns of the LSSPs. Compared with the LSSPs $TE_{1,1}$ mode, the dips of the LSSPs $TE_{2,1}$ and above as the quasi-BICs are much narrower, which indicates that their Q-factors are very high. A high Q-factor is an intrinsic advantage of the quasi-BICs because only little energy leaks and radiates out to

https://doi.org/10.1021/acsphotonics.2c00673
ACS Photonics XXXX, XXX, XXX−XXX

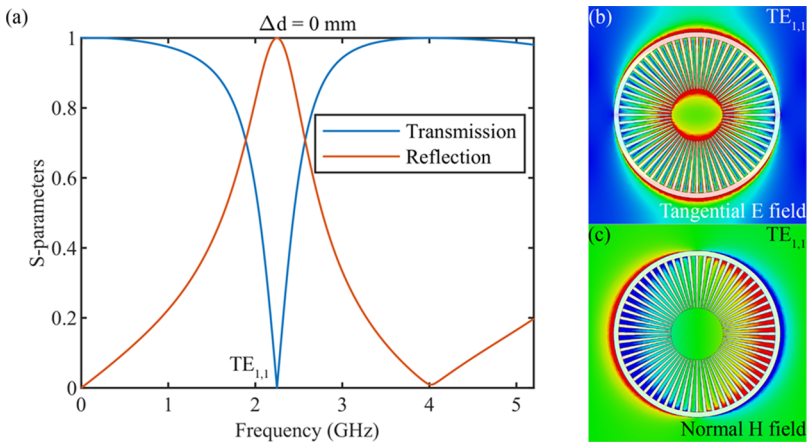

Figure 2. (a) Simulated S-parameters (linear scale) of the metasurface with concentric circular grating as the unit, including transmission and reflection amplitudes. (b) Electric and (c) magnetic field distributions of $TE_{1,1}$ mode.

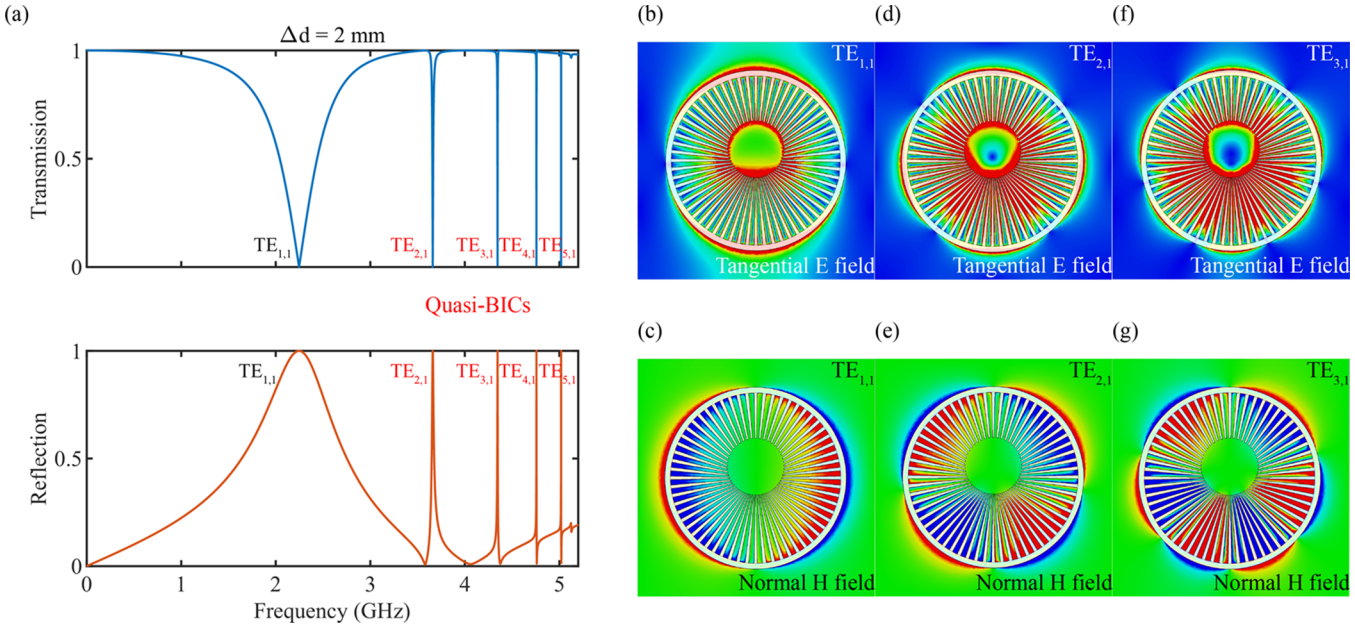

Figure 3. (a) Simulated S-parameters (linear scale) of the metasurface with eccentric circular grating as the unit, including transmission and reflection amplitudes. Quasi-BICs of the LSSPs are labeled in red. (b) Electric and (c) magnetic field distributions of $TE_{1,1}$ mode. (d) Electric and (e) magnetic field distributions of $TE_{2,1}$ mode. (f) Electric and (g) magnetic field distributions of $TE_{3,1}$ mode.

infinity, and most energy is confined on the gratings of the metasurface. In addition, by comparing the LSSPs $TE_{2,1}$ to $TE_{5,1}$ modes, which are all quasi-BICs, we find that the higher-order modes have narrower dips and thus have higher *Q*-factors.

***Q*-Factors of Quasi-BICs.** Taking LSSPs $TE_{2,1}$ mode under ideal conditions as an example, we study the behavior for the *Q*-factor of a quasi-BIC as a function of the asymmetry parameter. The transmission spectra of the LSSPs $TE_{2,1}$ mode with different displacements Δd are shown in Figure 4a. We observe that the true-BIC with a vanishing dip at $\Delta d = 0$ transforms into quasi-BIC, whose dip becomes wider and shifts to a lower frequency with the increase of Δd. The *Q*-factors of the quasi-BICs are finite; therefore, they can be calculated by $Q = f_0/\Delta f_{3dB}$, where f_0 is the resonant frequency and Δf_{3dB} is the 3-dB bandwidth.[14] Because the transmission spectra here are on the linear scale, the 3-dB bandwidth is replaced with the bandwidth with a transmissivity of 0.707. The *Q*-factors of the LSSPs $TE_{2,1}$ mode with displacements of 0.5, 1, 1.5, 2, and 2.5 mm are calculated to be 3837.34, 946.29, 426.57, 241.81, and 155.19, respectively. Therefore, a qualitative conclusion can be drawn from the calculated *Q*-factors that the *Q*-factor decreases with the increase in the displacement. Furthermore, a universal formula for the *Q*-factor of a quasi-BIC as a function of the asymmetry parameter has been derived[24]

$$Q = Q_0 \times \alpha^{-2} \tag{1}$$

where α is the asymmetry parameter and represents the displacement Δd in this study; Q_0 is a constant determined by the metasurface design, being independent on Δd. The formula presents that the *Q*-factor is inversely proportional to the square of Δd. Figure 4b shows a direct comparison of the value of the *Q*-factor of the $TE_{2,1}$ as a function of the displacement Δd for the metasurface with eccentric circular grating as the unit, which demonstrates the inverse square dependence of Δd. We can predict from the formula that the BICs are the limit case of $\Delta d = 0$ mm, in which the *Q*-factors become

https://doi.org/10.1021/acsphotonics.2c00673
ACS Photonics XXXX, XXX, XXX−XXX

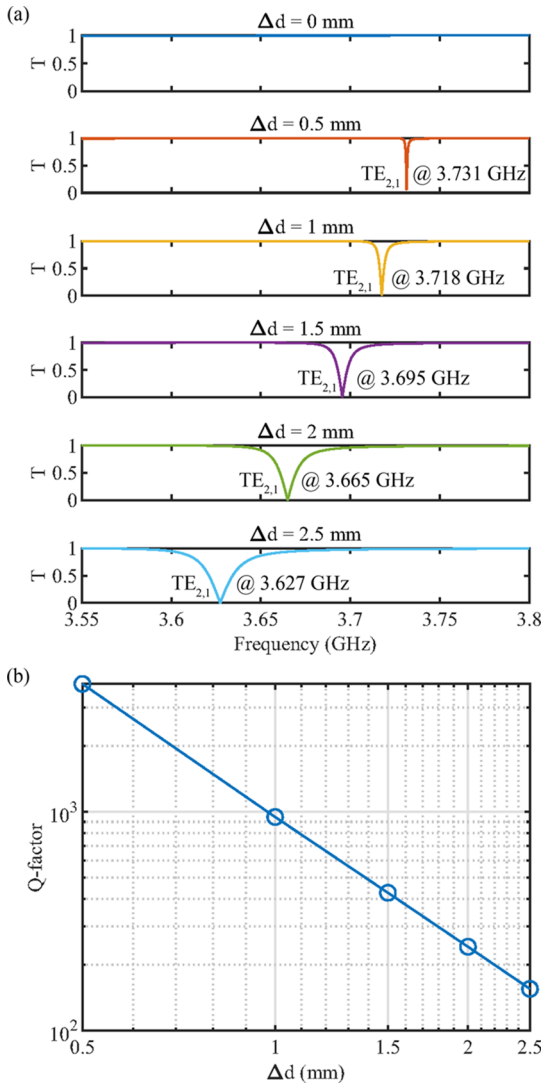

Figure 4. (a) Evolution of the transmission spectra (linear scale) near LSSPs $TE_{2,1}$ mode with the displacement Δd. (b) Dependence of the Q-factor on the displacement Δd (log–log scale).

infinity, the resonance widths become zero, and the LSSPs $TE_{2,1}$ and above vanish.

EXPERIMENTAL RESULTS

Observation of the Quasi-BICs of LSSPs. An experiment in the microwave band was carried out and the schematic of the experiment configuration is shown in Figure 5a. Two metasurfaces with Δd = 0 mm and Δd = 2 mm were manufactured, which are 10 × 5 arrays of circular gratings with an area of 42 cm × 21 cm. Both the concentric and eccentric circular gratings are made of copper with a thickness of 0.035 mm (1 oz). The dielectric substrate is Rogers RO4003C with a thickness of 0.508 mm, relative permittivity of 3.38, and loss tangent of 0.0027. In addition, organic solderability preservatives (OSPs) were applied to protect copper from oxidation or corrosion. A wooden base was used to fix the metasurfaces because wood has the advantages of low relative permittivity and low loss tangent and is transparent to the electromagnetic waves. Two ridged horn antennas with an operating frequency of 1–18 GHz were employed, one for emitting and one for receiving. They were fixed on a rotational platform specially made for the experiment. A vector network analyzer (VNA, model: Agilent N5245A) was employed to measure the S parameters, which sampled 6400 points equidistantly in the frequency range of 0–6 GHz.

A blank experiment was carried out first, in which nothing was placed between the ridged horn antennas. The spectrum is shown in Figure 5b as the reference of the transmission characteristic of the ridged horn antennas. Then, the metasurfaces with Δd = 0 mm and Δd = 2 mm were placed between the ridged horn antennas, respectively (Figure 5c, d). The normalized S_{21} spectra were calculated by subtracting the spectrum in the blank experiment from the spectra of the metasurfaces, the normalized S_{21} spectrum with Δd = 0 mm is shown in Figure 5e, and the normalized S_{21} spectrum with Δd = 2 mm is shown in Figure 5f with the quasi-BICs of the LSSPs labeled next to the dips in red. The experimental results are in good agreement with the simulation results, including the vanishing dips of the BICs (compare Figures 2a and 5e), the narrow dips of the quasi-BICs (compare Figures 3a and 5f), and the resonant frequencies of all the corresponding LSSPs modes. One difference is that the dips of the LSSPs $TE_{4,1}$ and above were not detected in the experiment, which is due to the material loss. (The material loss is discussed in detail in the "Discussion" Section.) The Q-factors of the LSSPs $TE_{1,1}$ and $TE_{2,1}$ modes can be calculated from the normalized S_{21} spectra, which are 4.06 and 214.80, respectively. As a quasi-BIC, the Q-factor of the $TE_{2,1}$ is much higher than that of the $TE_{1,1}$.

Comparison between Previous Studies. The quasi-BICs of the LSSPs in this study are compared with the previous studies in Table 1; all Q-factors compared are obtained experimentally. Because the LSSPs suffer from the relatively low Q-factors, many different excitation methods have been proposed to improve the Q-factors, such as excitation by monopole antennas,[6,7] plane waves,[16,18] spoof surface plasmons (SSPs),[12,38] microstrip lines,[13,39] magnetic couplers,[40] and so forth. The latter two are the state-of-the-art methods with high efficiencies, high Q-factors, and compatibility with printed circuit boards (PCBs). The Q-factors of the LSSPs coupled by microstrip lines can reach more than 100, and the Q-factors of the LSSPs excited by magnetic coupling can reach more than 200. In our previous work, multilayer structures of the circular gratings are adopted to reduce the radiation loss and a maximum Q-factor of 294.4 is obtained in the LSSPs $TE_{7,1}$ mode.[40] The starting point of both studies is to reduce the radiation loss because the material loss is inevitable. The structure presented in a previous study[16] is an array of ultrathin spirally corrugated metallic disks, which is like the array of concentric circular gratings in this work. Both structures have a rotational symmetry, on which only leaky $TE_{1,1}$ modes can be excited, and the Q-factors are both relatively low.

DISCUSSION

Effect of the Polarization Direction on the Quasi-BICs of the LSSPs. Because different polarization directions of the incident wave are the same for the concentric circular grating and the results are identical, we study the effect of the polarization direction on the quasi-BICs of the LSSPs on the metasurface with eccentric circular grating as the unit, and the results are shown in Figure 6. The schematic of the polarization direction is shown in Figure 6g; the polarization angle θ is defined as the angle between the polarization direction and the displacement Δd. θ = 0° is the case above.

https://doi.org/10.1021/acsphotonics.2c00673
ACS Photonics XXXX, XXX, XXX–XXX

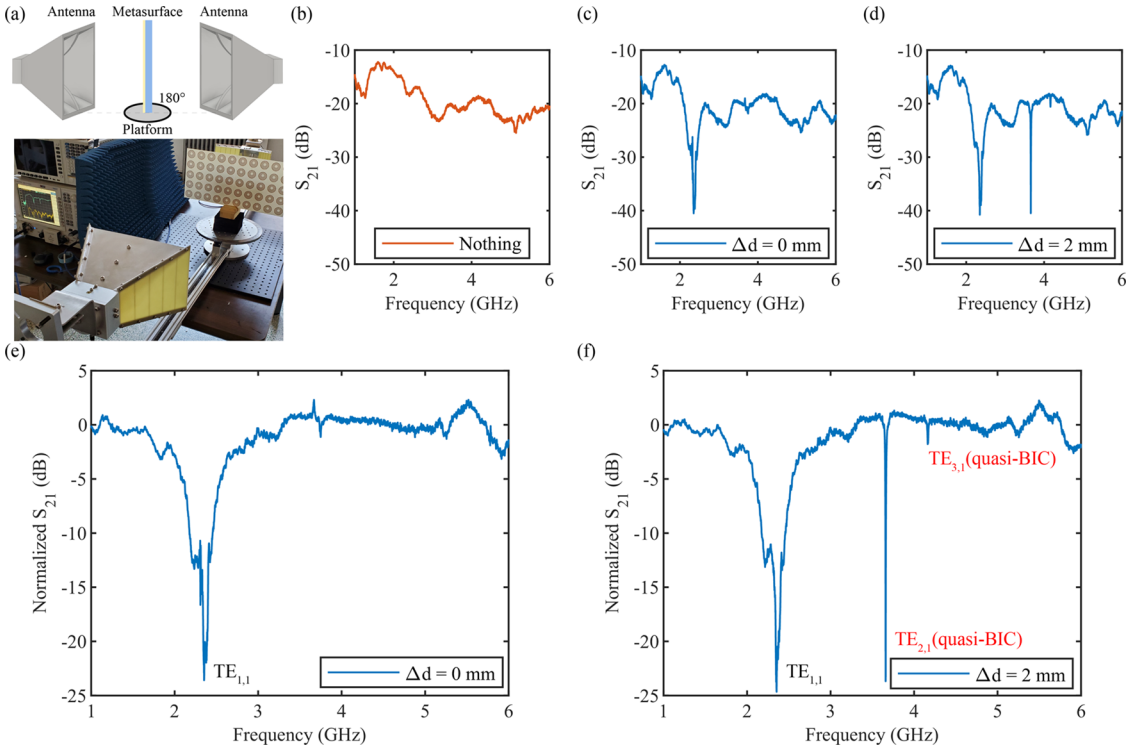

Figure 5. (a) Schematic of the experiment configuration and photograph of the experiment of the metasurface with Δd = 2 mm. The polarization direction of the electric field is the same as the direction of the displacement Δd. (b) Measured S_{21} spectrum in the blank experiment. (c) Measured S_{21} spectrum of the metasurface with Δd = 0 mm. (d) Measured S_{21} spectrum of the metasurface with Δd = 2 mm. (e) Normalized S_{21} spectrum of the metasurface with Δd = 0 mm, which was obtained by subtracting the spectrum in (b) from the spectrum in (c). (f) Normalized S_{21} spectrum of the metasurface with Δd = 2 mm, which was obtained by subtracting the spectrum in (b) from the spectrum in (d). (0−1 GHz, which is the cut-off frequency of the ridged horn antennas, is removed from the spectra.)

Table 1. Comparison with Previous Studies

refs	Q-factors	operating frequency	type (single/array)	excitation method
6	11.6[a]	1.18 GHz	single	monopole antenna
38	44.0[a]	9.9 GHz	single	SSPs line
39	69.6	3.41 GHz	single	microstrip line
13	104.8	1.5 GHz	single	microstrip line
40	294.4	5.3 GHz	single	magnetic coupler
16	7.3[a]	0.73 THz	array	plane wave
18	8.7 (bonding mode)	1.8 GHz (bonding mode)	array	plane wave
	32.6 (antibonding mode)	5.84 GHz (antibonding mode)		
quasi-BIC in this work	214.8	3.66 GHz	array	plane wave

[a]The data are calculated from line graphs.

The u-axis is established along the direction of the electric field, the v-axis is established along the direction of the magnetic field, and thus, the angle between the y-axis and the u-axis is θ.

When the plane wave with θ = 90° is incident, sharp LSSPs modes can be observed from Figure 6c,f. We use superscripts to distinguish different polarization directions, and we name the modes with θ = 0° as $TE_{2,1}^{(1)}$ and $TE_{3,1}^{(1)}$, and the modes with θ = 90° as $TE_{2,1}^{(2)}$ and $TE_{3,1}^{(2)}$. They are all quasi-BICs of the LSSPs formed by the symmetry broken. The electromagnetic field distributions of the $TE_{2,1}^{(2)}$ and $TE_{3,1}^{(2)}$ modes are shown in Figure 6h−k, and the electromagnetic field distributions of the $TE_{2,1}^{(1)}$ and $TE_{3,1}^{(1)}$ modes have been shown in Figure 3d−g; all of them present the patterns of the LSSPs. By comparing the corresponding modes with superscripts (1) and (2), we find that their patterns differ by 1/4 period in the azimuthal direction. It should be noted that they are not two degenerate modes, but two distinct modes with different resonant frequencies and different electromagnetic field distributions. Moreover, the mode with superscript (2) has a lower resonant frequency, narrower dip, and higher Q-factor.

In order to study the case of arbitrary polarization direction, θ = 45° is taken as an example. The S-parameters spectra are shown in Figure 6b, e, and both modes with superscripts (1) and (2) are successfully excited. In terms of resonant frequency, this case seems to be the superposition of the cases of θ = 0° and θ = 90°. However, complicated polarization conversion occurs, which is what we do not want. The amplitudes of copolarized (u-axis) and cross-polarized (v-axis) transmitted and reflected waves are all about 0.5. Therefore, the conclusion is that the metasurface can work when the electric or magnetic field of the plane wave is along the

https://doi.org/10.1021/acsphotonics.2c00673
ACS Photonics XXXX, XXX, XXX−XXX

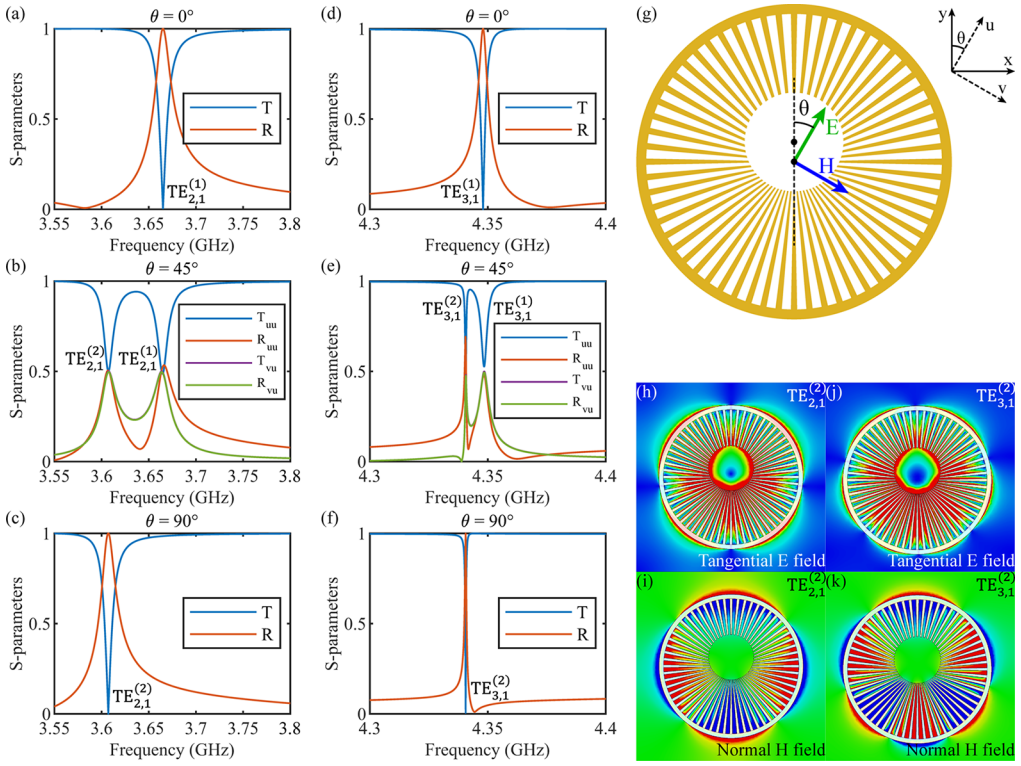

Figure 6. Simulated S-parameters (linear scale) near LSSPs $TE_{2,1}$ mode with (a) $\theta = 0°$, (b) $\theta = 45°$, and (c) $\theta = 90°$. Simulated S-parameters (linear scale) near LSSPs $TE_{3,1}$ mode with (d) $\theta = 0°$, (e) $\theta = 45°$, and (f) $\theta = 90°$. (For $\theta = 45°$, the spectra of T_{vu} and R_{vu} almost overlap.) (g) Schematic of the polarization direction of the incident wave. (h) Electric and (i) magnetic field distributions of $TE_{2,1}^{(2)}$ mode. (j) Electric and (k) magnetic field distributions of $TE_{3,1}^{(2)}$ mode.

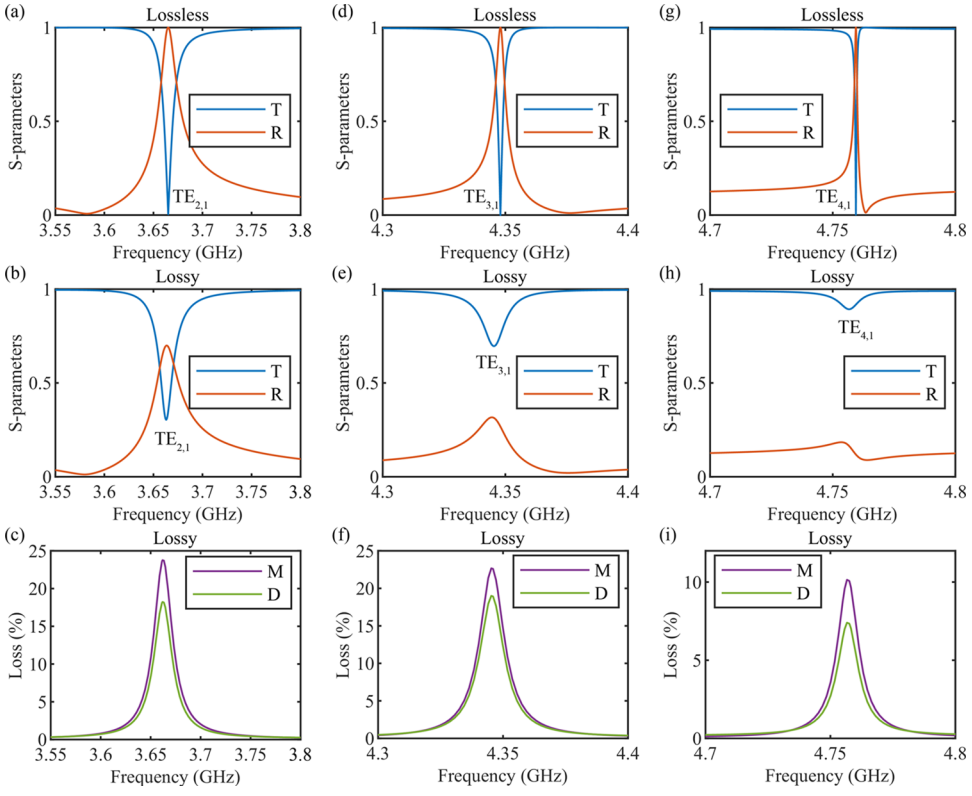

Figure 7. Simulated S-parameters (linear scale) near LSSPs $TE_{2,1}$ mode (a) with and (b) without material loss, near LSSPs $TE_{3,1}$ mode (d) with and (e) without material loss, and near LSSPs $TE_{4,1}$ mode (g) with or (h) without material loss. Spectra of energy loss near LSSPs (c) $TE_{2,1}$, (f) $TE_{3,1}$, and (i) $TE_{4,1}$ modes, in which "M" represents loss in metal and "D" represents loss in dielectric.

https://doi.org/10.1021/acsphotonics.2c00673
ACS Photonics XXXX, XXX, XXX−XXX

displacement Δd but is unavailable for other polarization directions.

Effect of the Material Loss on the Quasi-BICs of the LSSPs. In order to interpret the experimental results and to understand where the energy goes, the effect of the material loss was analyzed and the numerical simulation was done again with material loss considered. The loss tangent of the dielectric substrates was set as 0.0027, and the electric conductivity of the metal was set as 5.96×10^7 S/m; other simulation configurations were unchanged, Δd = 2 mm, θ = 0°. The simulation results in the lossy case are given in Figure 7, which agree well with the experimental results (compare Figures 5f and 7b,e,h).

In general, the material loss negatively affects the performance of the quasi-BICs of the LSSPs, which damps the resonances and broadens the spectra. Specifically, higher-order modes with narrower dips in the lossless case are more affected and the dip of the LSSPs $TE_{4,1}$ mode is almost flattened, which explains why the $TE_{4,1}$ and above vanished in the experiment, whereas the dip of the LSSPs $TE_{2,1}$ mode is still relatively sharp and the Q-factor of the $TE_{2,1}$ mode in the lossy case is calculated to be as high as 190.30, which is slightly smaller than the 241.81 in the lossless case and is close to the 214.80 in the experiment. For the LSSPs $TE_{2,1}$ mode, ∼50% of the energy is reflected, ∼10% of the energy is transmitted, and ∼40% of the energy is absorbed by the material, among which ∼23% of the energy is absorbed by the metal and ∼17% of the energy is absorbed by the dielectric. (The square of the S-parameter is proportional to the energy of the electromagnetic wave.) The loss in the metal is greater than that in the dielectric because the circular grating is a subwavelength structure and the surface currents that cause metal loss are distributed on all teeth.

CONCLUSIONS

In this study, quasi-BICs of the LSSPs were proposed and multiple LSSPs modes with high Q-factors were realized. The eccentric circular grating was designed as the unit of the metasurface, on which the LSSPs $TE_{2,1}$ and above turned into quasi-BICs from true-BICs, which were coupled to the plane wave and arose with weak energy leakage. In the experiment, narrow dips of the quasi-BICs of the LSSPs were observed, which is in good agreement with the simulation and demonstrates the feasibility of the scheme. The effects of the polarization direction and the material loss on the quasi-BICs of the LSSPs were discussed. This work greatly reduces the radiation loss of the LSSPs and improves the Q-factors of the LSSPs. We anticipate that our study will improve the performance of the applications based on the LSSPs, such as remote detection, high-precision spectroscopy, wireless sensing, and so forth.

AUTHOR INFORMATION

Corresponding Author

Chao-Hai Du − *Center for Carbon-Based Electronics and State Key Laboratory of Advanced Optical Communication Systems and Networks, School of Electronics, Peking University, Beijing 100871, China;* orcid.org/0000-0001-7970-9204; Email: duchaohai@pku.edu.cn

Authors

Si-Qi Li − *Center for Carbon-Based Electronics and State Key Laboratory of Advanced Optical Communication Systems and Networks, School of Electronics, Peking University, Beijing 100871, China;* orcid.org/0000-0003-2940-5821

Li-Zheng Yin − *State Key Laboratory of Advanced Optical Communication Systems and Networks, School of Electronics, Peking University, Beijing 100871, China;* orcid.org/0000-0003-3759-9849

Zi-Chao Gao − *State Key Laboratory of Advanced Optical Communication Systems and Networks, School of Electronics, Peking University, Beijing 100871, China*

Fan-Hong Li − *State Key Laboratory of Advanced Optical Communication Systems and Networks, School of Electronics, Peking University, Beijing 100871, China*

Complete contact information is available at: https://pubs.acs.org/10.1021/acsphotonics.2c00673

Author Contributions

The manuscript was written through contributions of all authors. All authors have given approval to the final version of the manuscript.

Funding

This work was supported in part by the National Natural Science Foundation of China (No. NSAF-U1830201), the Beijing Natural Science Foundation for Distinguished Young Scholars (No. JQ21011), and the National Key Research and Development Program of China (No. 2021YFA1600302). It was also supported in part by the Newton Advanced Fellowship from the Royal Society (No. NAF/R1/180121), United Kingdom.

Notes

The authors declare no competing financial interest.

ACKNOWLEDGMENTS

The authors are grateful to Prof. Fei Gao from Zhejiang University for useful discussions.

REFERENCES

(1) Prodan, E.; Radloff, C.; Halas, N. J.; Nordlander, P. A Hybridization Model for the Plasmon Response of Complex Nanostructures. *Science* **2003**, *302*, 419−422.

(2) Ozbay, E. Plasmonics: Merging Photonics and Electronics at Nanoscale Dimensions. *Science* **2006**, *311*, 189−193.

(3) Ma, R.-M.; Oulton, R. F.; Sorger, V. J.; Zhang, X. Plasmon lasers: coherent light source at molecular scales. *Laser Photonics Rev.* **2013**, *7*, 1−21.

(4) Garcia-Vidal, F. J.; Fernández-Domínguez, A. I.; Martin-Moreno, L.; Zhang, H. C.; Tang, W.; Peng, R.; Cui, T. J. Spoof surface plasmon photonics. *Rev. Mod. Phys.* **2022**, *94*, No. 025004.

(5) Pors, A.; Moreno, E.; Martin-Moreno, L.; Pendry, J. B.; Garcia-Vidal, F. J. Localized Spoof Plasmons Arise while Texturing Closed Surfaces. *Phys. Rev. Lett.* **2012**, *108*, No. 223905.

(6) Huidobro, P. A.; Shen, X.; Cuerda, J.; Moreno, E.; Martin-Moreno, L.; Garcia-Vidal, F. J.; Cui, T. J.; Pendry, J. B. Magnetic Localized Surface Plasmons. *Phys. Rev. X* **2014**, *4*, No. 021003.

(7) Shen, X.; Cui, T. J. Ultrathin plasmonic metamaterial for spoof localized surface plasmons. *Laser Photonics Rev.* **2014**, *8*, 137−145.

(8) Li, Z.; Xu, B.; Gu, C.; Ning, P.; Liu, L.; Niu, Z.; Zhao, Y. Localized spoof plasmons in closed textured cavities. *Appl. Phys. Lett.* **2014**, *104*, 251601.

(9) Gao, Z.; Gao, F.; Zhang, Y.; Zhang, B. Complementary structure for designer localized surface plasmons. *Appl. Phys. Lett.* **2015**, *107*, 191103.

(10) Liao, Z.; Fernández-Domínguez, A. I.; Zhang, J.; Maier, S. A.; Cui, T. J.; Luo, Y. Homogenous Metamaterial Description of

Localized Spoof Plasmons in Spiral Geometries. *ACS Photonics* **2016**, *3*, 1768−1775.
(11) Gao, F.; Gao, Z.; Luo, Y.; Zhang, B. Invisibility Dips of Near-Field Energy Transport in a Spoof Plasmonic Metadimer. *Adv. Funct. Mater.* **2016**, *26*, 8307−8312.
(12) Liao, Z.; Shen, X.; Pan, B. C.; Zhao, J.; Luo, Y.; Cui, T. J. Combined System for Efficient Excitation and Capture of LSP Resonances and Flexible Control of SPP Transmissions. *ACS Photonics* **2015**, *2*, 738−743.
(13) Zhang, X.; Cui, T. J. Deep-Subwavelength and High-Q Trapped Mode Induced by Symmetry-Broken in Toroidal Plasmonic Resonator. *IEEE Trans. Antennas Propag.* **2021**, *69*, 2122−2129.
(14) Zhang, X.; Cui, W. Y.; Lei, Y.; Zheng, X.; Zhang, J.; Cui, T. J. Spoof Localized Surface Plasmons for Sensing Applications. *Adv. Mater. Technol.* **2021**, *6*, No. 2000863.
(15) Zhang, X.; Bao, D.; Liu, J. F.; Cui, T. J. Wide-Bandpass Filtering Due to Multipole Resonances of Spoof Localized Surface Plasmons. *Ann. Phys.* **2018**, *530*, No. 1800207.
(16) Liao, Z.; Liu, S.; Ma, H. F.; Li, C.; Jin, B.; Cui, T. J. Electromagnetically induced transparency metamaterial based on spoof localized surface plasmons at terahertz frequencies. *Sci. Rep.* **2016**, *6*, 27596.
(17) Chen, L.; Xu, N.; Singh, L.; Cui, T.; Singh, R.; Zhu, Y.; Zhang, W. Defect-Induced Fano Resonances in Corrugated Plasmonic Metamaterials. *Adv. Opt. Mater.* **2017**, *5*, No. 1600960.
(18) Bao, D.; Cheng, Q.; Jiang, W. X.; Zhang, J. J.; Liao, Z.; Wu, J. W.; Yang, J.; Zhang, X. R.; Cui, T. J. Concentric designer plasmon hybridization in deep subwavelength metamaterial resonator. *Appl. Phys. Lett.* **2019**, *115*, 121103.
(19) Zhang, X.; Cui, T. J. Single-Particle Dichroism Using Orbital Angular Momentum in a Microwave Plasmonic Resonator. *ACS Photonics* **2020**, *7*, 3291−3297.
(20) Yin, J. Y.; Ren, J.; Zhang, L.; Li, H.; Cui, T. J. Microwave Vortex-Beam Emitter Based on Spoof Surface Plasmon Polaritons. *Laser Photonics Rev.* **2018**, *12*, No. 1600316.
(21) Gao, X.; Zhang, J.; Ma, Q.; Cui, W. Y.; Ren, Y.; Luo, Y.; Cui, T. J. Nonmagnetic Spoof Plasmonic Isolator Based on Parametric Amplification. *Laser Photonics Rev.* **2022**, *16*, No. 2100578.
(22) Gao, Z.; Gao, F.; Zhang, Y.; Zhang, B. Deep-subwavelength magnetic-coupling-dominant interaction among magnetic localized surface plasmons. *Phys. Rev. B* **2016**, *93*, No. 195410.
(23) Hsu, C. W.; Zhen, B.; Stone, A. D.; Joannopoulos, J. D.; Soljačić, M. Bound states in the continuum. *Nat. Rev. Mater.* **2016**, *1*, 16048.
(24) Koshelev, K.; Lepeshov, S.; Liu, M.; Bogdanov, A.; Kivshar, Y. Asymmetric Metasurfaces with High-Q Resonances Governed by Bound States in the Continuum. *Phys. Rev. Lett.* **2018**, *121*, No. 193903.
(25) Rybin, M.; Kivshar, Y. Supercavity lasing. *Nature* **2017**, *541*, 164−165.
(26) Fedotov, V. A.; Rose, M.; Prosvirnin, S. L.; Papasimakis, N.; Zheludev, N. I. Sharp Trapped-Mode Resonances in Planar Metamaterials with a Broken Structural Symmetry. *Phys. Rev. Lett.* **2007**, *99*, No. 147401.
(27) Campione, S.; Liu, S.; Basilio, L. I.; Warne, L. K.; Langston, W. L.; Luk, T. S.; Wendt, J. R.; Reno, J. L.; Keeler, G. A.; Brener, I.; et al. Broken Symmetry Dielectric Resonators for High Quality Factor Fano Metasurfaces. *ACS Photonics* **2016**, *3*, 2362−2367.
(28) Forouzmand, A.; Mosallaei, H. All-Dielectric C-Shaped Nanoantennas for Light Manipulation: Tailoring Both Magnetic and Electric Resonances to the Desire. *Adv. Opt. Mater.* **2017**, *5*, 1700147.
(29) Han, S.; Pitchappa, P.; Wang, W.; Srivastava, Y. K.; Rybin, M. V.; Singh, R. Extended Bound States in the Continuum with Symmetry-Broken Terahertz Dielectric Metasurfaces. *Adv. Opt. Mater.* **2021**, *9*, No. 2002001.
(30) Singh, R.; Al-Naib, I. A. I.; Yang, Y.; Chowdhury, D. R.; Cao, W.; Rockstuhl, C.; Ozaki, T.; Morandotti, R.; Zhang, W. Observing metamaterial induced transparency in individual Fano resonators with broken symmetry. *Appl. Phys. Lett.* **2011**, *99*, 201107.
(31) Zhang, F.; Huang, X.; Zhao, Q.; Chen, L.; Wang, Y.; Li, Q.; He, X.; Li, C.; Chen, K. Fano resonance of an asymmetric dielectric wire pair. *Appl. Phys. Lett.* **2014**, *105*, 172901.
(32) Karl, N.; Vabishchevich, P. P.; Liu, S.; Sinclair, M. B.; Keeler, G. A.; Peake, G. M.; Brener, I. All-optical tuning of symmetry protected quasi bound states in the continuum. *Appl. Phys. Lett.* **2019**, *115*, 141103.
(33) Wang, L.; Zhao, Z.; Du, M.; Qin, H.; Ako, R. T.; Sriram, S. Polarization insensitive symmetry protected quasi-bound states in the continuum at terahertz band. *J. Appl. Phys.* **2021**, *130*, 233102.
(34) Wang, M.; Li, B.; Wang, W. Symmetry-protected dual quasi-bound states in the continuum with high tunability in metasurface. *J. Opt.* **2020**, *22*, 125102.
(35) Maslova, E. E.; Rybin, M. V.; Bogdanov, A. A.; Sadrieva, Z. F. Bound states in the continuum in periodic structures with structural disorder. *Nanophotonics* **2021**, *10*, 4313−4321.
(36) Głowadzka, W.; Wasiak, M.; Czyszanowski, T. True- and quasi-bound states in the continuum in one-dimensional gratings with broken up-down mirror symmetry. *Nanophotonics* **2021**, *10*, 3979−3993.
(37) Algorri, J. F.; Dell'Olio, F.; Roldán-Varona, P.; Rodríguez-Cobo, L.; López-Higuera, J. M.; Sánchez-Pena, J. M.; Zografopoulos, D. C. Strongly resonant silicon slot metasurfaces with symmetry-protected bound states in the continuum. *Opt. Express* **2021**, *29*, 10374−10385.
(38) Su, H.; Shen, X.; Su, G.; Li, L.; Ding, J.; Liu, F.; Zhan, P.; Liu, Y.; Wang, Z. Efficient Generation of Microwave Plasmonic Vortices via a Single Deep-Subwavelength Meta-Particle. *Laser Photonics Rev.* **2018**, *12*, No. 1800010.
(39) Yang, B. J.; Zhou, Y. J.; Xiao, Q. X. Spoof localized surface plasmons in corrugated ring structures excited by microstrip line. *Opt. Express* **2015**, *23*, 21434−21442.
(40) Li, S.-Q.; Du, C.-H.; Han, F.-Y.; Li, F.-H.; Zhang, Z.-W.; Gao, Z.-C.; Liu, P.-K. Efficient magnetic-coupling excitation of LSSPs on high-Q multilayer planar-circular-grating resonators. *Opt. Express* **2021**, *29*, 25189−25201.

https://doi.org/10.1021/acsphotonics.2c00673
ACS Photonics XXXX, XXX, XXX−XXX